Published in final edited form as:
*Invest Ophthalmol Vis Sci*. 2006 July ; 47(7): 3109–3118. doi:10.1167/iovs.05-1397.

# Photoreceptor Organization and Rhythmic Phagocytosis in the Nile Rat *Arvicanthis Ansorgei*: A Novel Diurnal Rodent Model for the Study of Cone Pathophysiology

**Corina Bobu**[1], **Cheryl M. Craft**[2,3], **Mireille Masson-Pevet**[1], and **David Hicks**[1]

[1] Laboratoire de Neurobiologie des Rythmes, Université Louis Pasteur, Strasbourg, France

[2] Mary D. Allen Laboratory for Vision Research, Doheny Eye Institute, Los Angeles, California

[3] Department of Cell and Neurobiology, Keck School of Medicine, University of Southern California, Los Angeles, California

## Abstract

**Purpose—**To characterize rod and cone distribution, organization, and phagocytosis in the diurnal mouse-like rodent *Arvicanthis ansorgei*.

**Methods—**Retinas of adult *A. ansorgei* were processed for histology, electron microscopy and immunohistochemistry using rod- and mouse cone-specific antibodies. For phagocytosis studies, retinas were sampled every 3 hours under a 12-hour light–dark cycle and processed for double-label immunohistochemistry. The number of phagosomes in the retinal pigmented epithelium were quantified with a morphometric system.

**Results—***A. ansorgei* retinas were composed of 33% cones and 67% rods, approximately 10 times more cones than mice and rats. Cones were arranged in two cell layers at the scleral surface, distributed uniformly across the entire retina. Cone arrestin was distributed throughout the dark-adapted cones, from outer segments to synapses, whereas short- and mid-wavelength cone opsins were restricted to outer segments. Short-wavelength cone density was mapped in wholemounted retinas, in a significantly higher number in the central region. Rhodopsin immunopositive (rod) phagosomes showed a small peak late in the dark phase, then a large burst 1 to 2 hours after light onset, after decreasing to low baseline levels by 12 AM. Mid-wavelength cone opsin immunopositive (cone) phagosomes were 10 times less numerous than rods, and demonstrated a broad peak 1 to 2 hours after light onset.

**Conclusions—**The diurnal rodent *A. ansorgei* possesses a large number of cones, organized in a strict anatomic array. Rod and cone outer segment phagocytosis and shedding can be monitored simultaneously and show similar profiles but different amplitudes. This species may constitute a valuable novel animal model for investigating cone pathophysiology.

Phagocytosis of photoreceptor (PR) outer segment (OS) apical tips by the adjacent retinal pigmented epithelium (RPE) occurs throughout life and is an extremely elevated metabolic activity.[1–3] In the case of rods, continual synthesis of OS proteins and their insertion into nascent membranes at the basal surface of OS leads to apical displacement of older disc membranes.[4] To renew the phototransduction machinery while maintaining a constant OS length, apical packets of discs are shed and ingested by the RPE at a very high rate. It has been

Corresponding author: David Hicks Laboratoire de Neurobiologie des Rythmes, CNRS UMR 7168/LC2, INCI, 5 rue Blaise Pascal, 67084 Strasbourg Cedex, France; photoreceptor67@hotmail.com.

Disclosure: **C. Bobu**, None; **C.M. Craft**, None; **M. Masson-Pevet**, None; **D. Hicks**, None

estimated that each RPE cell in a person 80 years of age has internalized some 200 million discs.[5] In addition, phagocytic uptake of OS debris is not uniform, but exhibits a robust light-driven and/or circadian burst of activity near dawn.[6,7] Furthermore, other key features of PR function, including visual pigment synthesis,[8] OS turnover,[9] and ion channel sensitivity[10,11] exhibit strongly rhythmic activities. Several lines of experimental evidence, including temperature dependence, use of pharmacological inhibitors, and saturation curves of OS uptake,[12–14] indicate that rod OS phagocytosis involves a ligand-receptor interaction, and several different candidate receptors have been identified on the RPE apical surface. Recent work has identified the receptor tyrosine kinase c-Mer (MerTK) as critically involved in rod OS internalization,[15] and mutations in this protein are implicated in some forms of human retinal degeneration.[16] In addition, $\alpha V\beta 5$ integrin has been shown to be a component of the multimolecular complex controlling OS internalization.[17–19] However, virtually all of this information has been generated for rod PR, and knowledge of cellular and molecular mechanisms involved in cone OS phagocytosis is very limited. Although it was initially proposed that cone OS did not undergo phagocytosis in the same way as rods,[20] subsequent elegant morphologic studies have shown that these PRs did indeed shed apical packets of membrane that were ingested by the RPE.[21–25]

Cone PRs are responsible for color discrimination and visual acuity and are of utmost importance in human eyesight. The progressive loss of cone PRs represents the major source of visual handicap in a variety of retinal diseases, including retinitis pigmentosa and age-related macular degeneration (AMD).[26] The factors influencing cone survival are unknown, although we recently identified a diffusible factor produced by rods that may be critical for cones.[27] Perturbations in phagocytosis may well play a role in the development of AMD. It has been hypothesized that the progressive loss of vision associated with AMD could involve the impediment of phagocytosis through the accumulation of lipofuscin.[28]

One simple reason that has greatly hindered research on cone pathophysiology is the lack of a mammalian model permitting scrutiny under controlled experimental conditions. Conventional rodents (i.e., laboratory rats and mice) are nocturnal and have few cones (<3% of total PRs for mice[29] and <1% total PRs for rats[30]), whereas animals possessing cone-rich retinas—ground squirrels (approximately 90% cones[31]), chickens (approximately 65% cones[32]), and pigs (15%–20% cones[33])—exhibit various difficulties for experimentation, utilization of preexisting antibodies or databank sequences, or routine maintenance. Cone-rich transgenic mouse models have recently become available,[34] but the cones in such strains may not be fully normal (although recent data show that they display typical cone features by a wide range of structural and functional criteria.[35] We thus sought a species that would facilitate experimental research into cone function and survival and would allow us to examine cone phagocytosis specifically, through exhibiting certain key features: (1) a large percentage of easily identifiable cones; (2) diurnal behavior patterns similar to the human's; (3) genetic homology to mice for capitalizing on existing databases and antibody probes; (4) feasibility of monitoring behavior patterns and conducting in vivo experimentation; and (5) ease of maintenance and breeding in captivity. In this report, we present the initial characterization of such a species.

## Materials and Methods

### Animals

This study was conducted with Nile rats, *Arvicanthis ansorgei*, raised in our animal facilities from individuals captured in southern Mali in 1998.[36] Since this time, the colony has been maintained on a 12-hour light–dark (LD) cycle in an ambient temperature of 22 ± 1°C. A total of 40 animals were used, all females, with most experiments involving young adults (5–7 months), with some individuals up to 26 months. The animals were supplied ad libitum with

water and standard rat chow. Animal treatment and experimentation adhered to the guidelines in the ARVO Statement for the Use of Animals in Ophthalmic and Vision Research.

### Histology and Retinal Ultrastructure

For examination of the *A. ansorgei* retina by light and electron microscopy for histologic analysis, eyes were removed from euthanatized animals; fixed in 4% paraformaldehyde, 0.1% glutaraldehyde, and 0.1 M phosphate-buffered saline (PBS; pH 7.4) for 3 hours; and washed in 0.1 M PBS overnight at 4°C. The tissue was postfixed for 1 hour at 4°C in 2% osmium tetroxide in rinse buffer. Dehydration, infiltration with Epon resin, and polymerization of samples was performed by conventional methods. Ultrathin sections (70–90 nm) were cut on a microtome (Ultracut; Leica, Heidelberg, Germany), collected on grids, and counterstained successively in 1% aqueous uranyl acetate and 1% aqueous lead citrate for 2 minutes each. Sections were finally washed, dried, and examined by transmission electron microscope (model EM 208; Philips Eindhoven, The Netherlands). Semithin sections (0.5 $\mu$m) were collected on glass slides, and stained with 1% toluidine blue in 1% aqueous sodium tetraborate for 1 minute.

### Western Blot Analysis

To ensure correct cross-reactivity of the different antibodies, we ran Western blots for each on extracts prepared from *A. ansorgei* and rat (*Rattus norvegicus*) retinas (two retinas from each). Retinas were collected and homogenized in lysis buffer (20 mM Tris-HCl [pH 7.4], 150 mM NaCl, 1% Triton X-100, 0.1% SDS, 1 mM EDTA) containing a protease inhibitor cocktail (Roche Molecular Biochemicals, Meylan, France). Measurement of total protein concentrations in aliquots from each sample gave values of 18 mg/mL for the rat and 18.8 mg/mL for *A. ansorgei*. Proteins (15 $\mu$L/well) were separated by 10% SDS-poly-acrylamide gel electrophoresis and transferred to nitrocellulose membranes with a semidry blotter (Bio-Rad, Munich, Germany). The membranes were blocked with TBS containing 0.1% Tween 20 and 3% fat-free powdered milk (pH 7.3) for 1 hour at room temperature. Membranes were incubated with the following primary antibodies: monoclonal anti-rhodopsin antibody Rho-4D2,[37] polyclonal anti-mouse mid-wavelength (MW)-cone and short-wavelength (SW)-cone opsins,[38] and polyclonal anti-mouse cone arrestin.[39] Each primary antibody was diluted to a final concentration of ~0.1 $\mu$g/mL (1:10,000 dilutions of ascites fluid or antiserum, respectively) and incubated overnight at 4°C, the membranes were washed thoroughly and then incubated with goat anti-mouse or goat anti-rabbit IgG-horseradish peroxidase secondary antibodies (1:20,000; Jackson ImmunoResearch Laboratories, West Grove, PA). Immunoreactive bands were visualized with chemiluminescence (Super Signal ECL kit; West Pico; Pierce, Rockford, IL), according to the manufacturer's instructions. Apparent molecular masses were estimated by comparison to prestained molecular size markers (Invitrogen-Life Technologies, Gaithersburg, MD). Western blot analyses were performed for each antibody in two independent experiments, and representative images are shown.

### Immunohistochemistry

Eyes were fixed overnight in 4% paraformaldehyde at 4°C, transferred to an ascending series of sucrose solutions (10%, 20%, and 30%, each for 2 hours) and embedded (Tissue-Tek; Sakura Fintek, Tokyo, Japan), and 18-$\mu$m-thick cryostat sections were prepared and stored at −20°C until ready for use. The sections were permeabilized with Triton X-100 (0.1% in PBS for 5 minutes) and then saturated with PBS containing 0.1% BSA, 0.1% Tween-20, and 0.1% sodium azide (buffer A) for 30 minutes. Sections were incubated overnight at 4°C with the following primary antibodies diluted in buffer A. Antibodies used were monoclonal anti-rhodopsin antibody Rho-4D2, polyclonal anti-mouse MW-cone and SW-cone opsins, polyclonal anti-mouse cone arrestin, and monoclonal anti-RPE65[40] (Chemicon International Ltd., Temecula, CA). Secondary antibody incubation was performed at room temperature for 2 hours with

Alexa (488 or 594) goat anti-rabbit or anti-mouse IgG-conjugated antibodies (Invitrogen, Eugene, OR). Cell nuclei were stained with 4,6-diamino-phenyl-indolamine (DAPI; Invitrogen). Slides were washed thoroughly, mounted in PBS and glycerol (1:1), and observed with a confocal laser scanning microscope (LSM 510 ver. 2.5; Carl Zeiss Meditec, Jena, Germany), a scanning device mounted on an inverted microscope (Axiovert 100; Carl Zeiss Meditec), or a fluorescence microscope (Optiphot 2; Nikon, Melville, NY) equipped with differential interference contrast optics. Images were relayed by charge-coupled device (CCD) camera video capture to a dedicated computer containing image analysis software (Visiolab; Biocom, Lyon, France).

### Retinal Wholemount Immunohistochemistry

Two eyes were used to prepare retinal wholemounts. Before enucleation, a small incision was made in the dorsal margin of the ora serrata for orientation. Retinas were carefully dissected to preserve orientation; fixed in 4% paraformaldehyde, PBS, and 5% sucrose for 4 hours at room temperature; washed with 0.1 M Tris-buffered saline (pH 7.4; TBS) and water (5 minutes each), and dip frozen in chilled acetone (−20°C for 5 minutes). After washes in water and TBS (5 minutes each), the retinas were incubated for 2 hours in 10% $H_2O_2$ in PBS with 1 drop of 30% ammonia to bleach pigment granules in the RPE and visualize the retina more clearly. The retinas were then washed with PBS and permeabilized in 0.3% Triton X-100 for 1 hour and saturated in blocking buffer overnight and incubated with either rho-4D2 or anti-SW-cone opsin antibodies for 1 day at ambient temperature. After extensive washing (8 hours with six changes of buffer), the retinas were incubated with the corresponding secondary antibody for 24 hours at 4°C, cut into four quadrants (dorsal, ventral, temporal, and nasal), using the initial incision as a reference, and flattened under coverslips in 1:1 PBS-glycerol. For quantification at each of the selected retinal locations, tissue was divided into near (within 1.5 mm of the optic nerve head), mid (1.5–3 mm from the optic nerve head), and far (>3 mm from the optic nerve head) regions for each of the four quadrants, and blue cone densities were estimated for each zone by counting the average number of SW cones in 20 randomly chosen 150 × 150-$\mu$m fields viewed with a 40× objective lens. Because total cell-packing density did not differ greatly across the retina, these values are expressed as the mean number per field.

### Quantification of Phagocytosis during the Light–Dark Cycle

Animals used to study temporal variations in phagocytosis were euthanized every 3 hours during the 12-hour light–dark cycle ($n = 4$ for each time point). According to the 24-hour clock, lights were turned on at 0800 hours (8 AM) and off at 2000 hours (8 PM), and animals were killed at midnight (2400 hours) and 0300, 0600, 0900, 1200, 1500, 1800, and 2100 hours. Eyes were rapidly removed and fixed in 4% paraformaldehyde, as described earlier. For samples taken during the dark phase, enucleation was performed under dim red light illumination. Sections were obtained across the whole width of the retina, from the superior to inferior margin, passing within 1 mm of the optic nerve head. Four sections from one eye of each animal at each point were analyzed (i.e., a total of 16 sections per time point). They were immunostained as detailed herein, using either rho-4D2 (rods) or anti-MW-cone opsin (MW cones). OS staining of both PR populations was very regular, the leading edge forming a straight border. Taking this edge as a baseline, any immunopositive inclusion of ≥1 $\mu$m lying within the RPE subcellular space (visualized by faint background lighting) was scored as a phagosome. Counting of phagosomes was achieved by aligning a 150 × 150-$\mu$m grid placed within the eyepiece, parallel with the RPE layer. Taking the optic nerve head as reference, the grid was displaced dorsally and ventrally along the OS/RPE interface, from the posterior to the superior margin. In this way, the RPE was sampled across the entire width of each eye.

### Statistics

For statistical analysis of SW-cone densities and phagosome uptake, we used a one-way analysis of variance (ANOVA) followed by an ad hoc Fisher least-significant difference test, with acceptance levels of $P < 0.05$.

## Results

### Morphologic Characterization of the Retina of *A. ansorgei*

The retinal morphology of *Arvicanthis* represented in Figure 1 shows a typical tiered structure. The RPE is visible as a clear basal region containing nuclei and mitochondria, and a heavily pigmented apical area packed with melanin granules. Within the outer nuclear layer (ONL), nuclei of cone PRs can be distinguished from those of rods by the less-intense staining, corresponding to less-condensed heterochromatin.

At the ultrastructural level, the RPE–OS interface demonstrated an orderly arrangement of rod and cone OS apposed to the RPE apical surface (Fig. 2). Rod OS appeared as cylindrical structures, the stacked discs clearly visible. Cone OS were narrower and tapered, slightly more electron dense, with areas of clear cytoplasm and surrounding cone matrix sheath. RPE exhibited many melanin granules positioned within the apical region. Occasional phagosomes of rod or cone origin were equally visible (Fig. 2A, arrows). Individual RPE cells were in contact with both rod and cone OS.

### Western Blot Analysis of PR Antibodies

We performed comparisons of the different PR antibodies between rat and *Arvicanthis* whole retinal extracts. As shown in Figure 3, each antibody gave similar results in terms of the apparent molecular mass species detected: MW-cone opsin immunoreactivity was observed at ~40 kDa, a faint band in the rat retina but a much more intense signal in the *Arvicanthis* retina (Fig. 3A; lanes 1, 2). SW-cone opsin immunoreactivity was seen at the same size range (~40 kDa) and was approximately of equal intensity in both rodents (Fig. 3A, lanes 3, 4); cone arrestin immunoreactivity was detected at ~48 kDa, being very faint in the rat and strong in the *Arvicanthis* (Fig. 3A, lanes 5, 6). Rho-4D2 anti-rod opsin immunoblots were performed in two different conditions, using heated and unheated samples. In both rodents, rod opsin immunostaining was generally comparable, although somewhat less intense in the *Arvicanthis*. Boiled samples contained immunoreactive bands at 54, 80, 115, and >140 kDa (Fig. 3B, lanes 1, 3), and unheated samples also showed strong staining of a band at ~34 kDa (Fig. 3B, lanes 2, 4). These immunoblot data provided evidence for correct cross-reactivity of the different antibodies between the rodent species.

### Rod and Cone Immunohistochemistry

Immunolabeling of the *A. ansorgei* retina was performed with different rod and cone antibody markers. Anti-mouse MW-cone opsin stained abundant OS, forming a dense continuous band of label across the retina (Figs. 4A, 4B). There was no antibody binding detectable in other cellular locations. Anti-mouse SW-cone opsin labeled only a few small structures within the OS (Figs. 4C, 4D). By contrast, in sections obtained from dark-adapted animals, anti-mouse cone arrestin produced intense staining throughout the cone cells, filling the OS and cell bodies within the uppermost two layers of the ONL and extending down their axons to the synaptic pedicles (Figs. 4E, 4F). Rhodopsin immunostaining produced an intense signal in the OS, forming a somewhat broader band than that observed for MW-cone opsin, and in addition outlined rod cell bodies in the inner two-thirds of the ONL (Fig. 5). These data show that the ONL is separated into a distal region composed exclusively of cone cell bodies (two rows) and an inner region composed exclusively of rod cell bodies (four rows). This anatomy was

apparent uniformly across the retina, from center to mid periphery, but toward the far periphery, the ONL thinned to four to five cell bodies, with only a single distal row of cones, and three to four rows of rods (not shown).

We also immunolabeled frozen sections of *A. ansorgei* eyes with anti-RPE65 monoclonal antibody. As seen in Figure 6, antibody staining was intense and specific within the RPE layer.

### Wholemount Immunolabeling of *A. ansorgei* Retina

To obtain a more comprehensive distribution pattern of SW cones, we performed immunostaining of flatmounted retinas (Fig. 7A). Whereas rod opsin flatmount labeling revealed numerous immunopositive OS throughout the retinal fields (data not shown), SW cones were sparsely distributed across the retinal surface. The distribution pattern is shown in Figure 7B, mapped against a camera lucida depiction of the retina, and in histogram form for each of the 12 regions analyzed (Fig. 7C). There were no significant differences in the number of SW cones between left and right eyes (not shown) or between any of the four quadrants or the superior and inferior hemispheres, but cone density was significantly higher in the central annulus than in the far periphery (an overall threefold difference; $P < 0.001$). There were also significantly higher densities in the mid periphery than in the far periphery ($P < 0.01$).

### Daily Rhythms in Rod and Cone Phagocytosis

Immunoreactive rod or cone debris were identifiable unambiguously within the RPE cytoplasm. An examination of sections obtained at different time points within the standard 12-hour light–dark cycle revealed the presence of inclusions labeled with rod opsin antibody at 0900 hours (1 hour after light onset), but not at 2100 (1 hour after light offset; Figs. 8A, 8B). Similar analyses using an MW-cone opsin antibody showed a similar profile: immunopositive inclusions were reproducibly seen at 0900 but not at 2100 hours (Figs. 8C–F). Simultaneous visualization of both rod and cone phagosomes at 0900 hours did not reveal any obvious association between the two populations, although they were clearly both present within individual RPE cells (Fig. 9). Given the low number of SW-cones we did not attempt to examine phagocytosis in this subpopulation.

Quantification of rod and cone phagosomes was performed throughout the light–dark cycle. These analyses confirmed the rhythmic nature of phagocytic uptake of both populations and revealed that the two profiles were largely similar (Fig. 10). Both showed large peaks of phagosome numbers at around 0900 hours, significantly different from all other time points. A second smaller peak was also visible for rod phagosomes, centered on 0300 hours but detectable at both 2400 and 0600 compared with the minimum values observed at 1800 and 2100 hours (Fig. 10A). The number of cone phagosomes was always much lower than rods, by a factor of 10 (Fig. 10B). Phagosomal activity was, however, quite variable, since at any given time the number of phagosomes generally varied by a factor of 2 between individual animals and sometimes by as much as 10-fold. In addition, these differences were not consistent with respect to rods or cones (i.e., animals showing the lowest number of rod phagosomes did not necessarily also exhibit a low number of cone phagosomes; Table 1). There was some correspondence between a low number of phagosomes and age, since the two lowest values for both rod and cone phagosomes were observed in the two oldest individuals (Table 1).

## Discussion

We present the initial characterization of a diurnal murine rodent with respect to PR phenotype, distribution, and rhythmic phagocytosis. The data show that cones form a large percentage of total PRs, approximately 33%, and that they undergo cyclic phagocytic turnover in a general pattern similar to that of rods.

Rodent species typically used for experimental research, namely laboratory rats (*Rattus norvegicus*) and mice (*Mus musculus*), have an important drawback for investigations directed at cone pathophysiology. These naturally nocturnal animals have a very low number of cones (estimated at 2.8% total PRs for mice[29] and <1% for rats[30]). Although this has not prevented the study of cone differentiation,[41] phenotype,[42] function,[43] and degeneration[44,45] in these species, it has nevertheless hindered cell biological studies. For example, very little information is currently available on direct effects of neurotrophic factors or environmental insults (e.g., intense light exposure) on cone survival.[46,47] There are some "higher" animal models for studying cone PRs, such as chickens (>60% cones[32]), pigs (15%–20%[33]), and ground squirrels (>90%[31]). These animals have aided in exploring PR differentiation,[48] cone degeneration,[49] trophic factor effects,[50] turnover,[51] and cone-specific circuitry.[52] These models present certain drawbacks, however, such as difficulties in husbandry or surgery, routine breeding in captivity, and lack of genetic information and molecular probes. In searching for an animal model that would facilitate cell biological examination of cones, we wanted to retain as far as possible the advantages of small rodents (ease of handling and housing, large litter sizes, and feasibility of performing surgery), combined with a phylogenetic match to laboratory mice for optimizing exploitation of preexisting databanks and available antibody probes (although it should be noted that techniques such as siRNA require a perfect match and may not be straightforward to perform). The Nile rat genus *Arvicanthis* appeared a promising candidate, since it belongs to the Muridae family, can be maintained as a stable colony in captivity, and has a diurnal behavior pattern. This genus has been extensively studied as a model for the relationship between circadian clock gene expression, suprachiasmatic nucleus function, and diurnal behavior.[36,53–59] Despite the implication of photic stimuli in regulation of activity,[59,60] to the best of our knowledge, there are no published data referring to retinal neuroanatomy.

All tested antibodies, raised against either mouse or rat sequences of retinal proteins, cross-reacted fully with *Arvicanthis*. The anti-mouse cone arrestin antibody demonstrated a very similar subcellular distribution in dark-adapted *Arvicanthis* retinal sections (Fig. 4) compared with those obtained from dark-adapted mice.[39] We conducted mapping studies of SW-cones across the entire retina, since it has been reported that the two cone spectral classes present in lower mammals are distributed in a heterogeneous pattern, with SW-cones predominantly located in the ventral field.[61,62] Although we observed a significantly higher number of SW cones in the central field than in the far periphery, there was no detectable variation in their number as a function of retinal quadrant. Relatively homogenous distributions have also been seen in other murine genera.[63] Although we did not perform similar fine mapping studies for MW cones, analysis of a large number of sections taken across all retinal areas did not reveal major differences (data not shown). Western blot comparisons of relative abundance of MW-cone opsin and cone arrestin between rats and *Arvicanthis* showed expected large excesses for the latter species; unexpectedly, the abundance of SW-cone opsin appeared virtually identical between the two. This similarity is presumably due to a low SW- to MW-cone ratio, a lower amount of SW-cone opsin per cell, or both. Electrophoretic separation of rhodopsin frequently produces multimeric aggregates, especially on heating of samples under non-reducing conditions which converts virtually all monomeric forms into dimers or higher complexes.[64,65] We used this anomalous electrophoretic migration behavior to underline that rhodopsin antibody specificity was retained for *Arvicanthis*. The intensity of bands was noticeably fainter in *Arvicanthis* preparations, consistent with the reduced rod population.

An important aspect that has been difficult to study in mammals concerns cone phagocytosis by the apposing RPE. Autoradiographic studies led to the conclusions that protein (mainly opsin) synthesis occurred in the inner segment and that newly synthesized membranes (i.e., discs) were displaced apically by continuous addition at the basal surface of the OS.[1–3] Since this time, extensive data have been gathered concerning the chain of events linking OS shedding and their subsequent internalization by the RPE. Initially, OS bind to the RPE apical surface,

triggering activation of an intracellular second-messenger cascade, which in turn activates the ingestion of bound OS. CD36, MerTK, and $\alpha V\beta 5$-integrin receptors have all been implicated as playing crucial roles in phagocytosis. The macrophage scavenger receptor CD36 was found to regulate the rate of OS internalization.[18] Binding of OS to the receptor tyrosine kinase c-Mer (MerTK) leads to phosphorylation and activation of the second-messenger cascade.[15,66,67] Binding of OS requires the activation of $\alpha V\beta 5$-integrin receptors, which interact with MerTK via the focal adhesion kinase (FAK) signaling pathway.[66] In brief, OS binding to $\alpha V\beta 5$-integrin receptors activates FAK, which in turn phosphorylates MerTK, leading to activation of the second-messenger cascade. Finally, the specific ligand for MerTK is growth-arrest–specific protein 6, which is necessary for OS phagocytosis.[68] Perturbation in the phagocytosis pathway can lead to retinal degeneration, as observed in the RCS rat[15] and a subset of patients with retinitis pigmentosa.[16]

These molecular details are only known for certain for rod uptake. Contrary to rods, cones appeared to be more static elements, since they did not exhibit a band of radioactivity—rather diffuse labeling of the OS.[4,20,69] However, phagocytic uptake of shed cone membrane debris was described in the cone-dominated retinas of lizards[70] and squirrels.[21,51] This latter group also observed unequivocal cone OS uptake in cats,[25] monkeys[23,24] and humans.[22] An important goal of the present study was to quantify rod and cone phagocytosis as a function of daily time. Previous investigations have shown a strong rhythmic component of phagosome uptake, entrained by day/night alternation and/or circadian control. In all nocturnal and diurnal vertebrates examined, both cold- and warm-blooded, rod OS uptake occurs maximally at or shortly after light onset. In rats, this daily rhythm is established by 2 weeks of age and is irrespective of the lighting conditions during development.[71] It persists for up to 14 days in constant darkness and is independent from the brain's biological clock,[6,7] since it is maintained after optic nerve section or destruction of the suprachiasmatic nucleus.[72,73] Thus, an intrinsic oscillator exists within the eye, although feedback from the brain is needed to synchronize the circadian shedding rhythm with the day–night cycle.[74] The timing of cone shedding is more variable, since in most species (goldfish,[75] lizards,[70] chickens,[76] and tree squirrels[21]) it occurs during the night time, whereas in rhesus monkeys,[24] tree shrews,[77] and cats[25] rod and cone OS shedding both occur maximally just after light onset. The data from *Arvicanthis* resemble those obtained in cats in several respects: (1) Rod and cone shedding occur together shortly after light onset. Although there are large differences between the animals in lifestyles and retinal anatomy (there is no obvious area centralis in Nile rats), *Arvicanthis* represents a further example of maximum cone shedding occurring at light onset. The four mammalian species in which such dynamics are observed are all active during the day. (2) There is a secondary, smaller increase in rod shedding late during the night period. This smaller peak occurred around the same time in both animals (~6 to 8 hours after light offset). (3) The maximum number of rod phagosomes greatly exceeds that of cones. In both species rod phagosomes outnumbered cone phagosomes by a factor of 10. This may reflect the different turnover rates of rods versus cones, because rod membranes are thought to be renewed more rapidly than cones.[20,69] However, there is controversy over the issue, and estimates in the cat give similar values for both PR types.[25] (4) Variability in the number of phagosomes between individuals was observed at any given time point. This variability was also seen in cats, and, as in this study, differences between individuals were not consistent (i.e., those showing a high number of rod phagosomes could exhibit a low number of cones, and vice versa). One source of variation could be age, since the eldest animals showed the lowest number of inclusions. We are currently performing similar analyses under constant dark conditions to see whether rod and/or cone phagocytosis are circadian or light driven.

The methodological approach used herein to quantify rod and cone phagosomes differs from that used in previous studies. Whereas purely morphologic criteria have been used by other workers, we exploited the availability of rod- and cone-specific immunologic probes to map

simultaneously the appearance and distribution of both populations. In distinguishing rod from cone phagosomes, previous studies have relied on species exhibiting large cone OS, or regional specializations (macula or area centralis). Rodents possess small, narrow cone OS, and similar approaches would not be feasible. The use of antibodies directed against the integral membrane protein visual pigments has the advantage of allowing screening of a large number of sections and of performing ultrastructural immunohistochemistry. Rhodopsin antibodies have been used previously to examine rod-derived phagosomes in the RPE at the electron microscope level.[78] An important caveat is that the epitopes recognized by each antibody will be destroyed during the enzymatic degradative process, and hence do not allow us to observe phagolysosome metabolism. We also noted that cone arrestin antibodies did not label phagosomes, presumably because the cytoplasmic antigen leaks rapidly from incipient phagosomes (data not shown). Finally, we made no distinction between "shedding" and "phagosomes," since our counting procedure would have excluded incipient packets of discs present outside the RPE.

In conclusion, we present the initial characterization of a diurnal mouselike rodent with a large number of histologically and immunologically identifiable cones. We have mapped rod and cone distribution and composition and quantified rod and cone phagosome uptake as a function of daily time. Our future studies will focus on cone phagocytosis, of particular importance with respect to human macular function and health and possibly centrally involved in the progression of macular degeneration.[28]

## Acknowledgments

The authors thank Guy Normand and Claudine Boissier for assistance with the Western blot analyses, Jorgé Mendoza for advice on statistical analysis methods, and Xuemei Zhu and Bruce Brown for cone antibody characterization.

Supported by a grant from Retina France (CB); and, in part, by the Mary D. Allen Endowment, and National Eye Institute (NEI) Grant EY015851, NEI core Grant EY03040 to the Doheny Eye Institute, and Research to Prevent Blindness. CMC holds the Mary D. Allen Chair in Vision Research.

## References

1. Young RW. The renewal of photoreceptor cell outer segments. J Cell Biol 1967;33:61–72. [PubMed: 6033942]
2. Young RW, Bok D. Participation of the retinal pigment epithelium in the rod outer segment renewal process. J Cell Biol 1969;42:392–403. [PubMed: 5792328]
3. Bok D, Young RW. The renewal of diffusely distributed protein in the outer segments of rods and cones. Vision Res 1972;12:161–168. [PubMed: 4537522]
4. Young RW, Droz B. The renewal of protein in retinal rods and cones. J Cell Biol 1968;39:169–184. [PubMed: 5692679]
5. Young RW. Biological renewal; applications to the eye. Trans Ophthalmol Soc UK 1982;102:42–75. [PubMed: 6963064]
6. LaVail MM. Rod outer segment disc shedding in relation to cyclic lighting. Exp Eye Res 1976;23:277–280. [PubMed: 987920]
7. LaVail MM. Circadian nature of rod outer segment disc shedding in the rat. Invest Ophthalmol Vis Sci 1980;19:407–411. [PubMed: 7358492]
8. Von Schantz M, Lucas RJ, Foster RG. Circadian oscillation of photopigment transcript levels in the mouse retina. Brain Res Mol Brain Res 1999;72:108–114. [PubMed: 10521605]
9. Cahill GM, Besharse JC. Circadian clock functions localized in Xenopus retinal photoreceptors. Neuron 1993;10:573–577. [PubMed: 8476609]
10. Ko GYP, Ko ML, Dryer SE. Circadian regulation of cGMP-gated cationic channels of chick retinal cones: role of Erk MAP kinase and $Ca^{2+}$/calmodulin-dependent kinase-II. Neuron 2001;29:255–266. [PubMed: 11182096]

11. Lu J, Zoran MJ, Cassone VM. Daily and circadian variation in the electroretinogram of the domestic fowl: effects of melatonin. Vision Res 1991;31:717–734. [PubMed: 1843772]
12. Mayerson PL, Hall MO. Rat retinal pigment epithelial cells show specificity of phagocytosis in vitro. J Cell Biol 1986;103:299–308. [PubMed: 3522605]
13. Hall MO, Abrams T. Kinetic studies of rod outer segment binding and ingestion by cultured rat RPE cells. Exp Eye Res 1987;45:907–922. [PubMed: 2828096]
14. Hall MO, Abrams TA, Mittag TW. ROS ingestion by RPE cells is turned off by increased protein kinase C activity and by increased calcium. Exp Eye Res 1991;52:591–598. [PubMed: 2065727]
15. D'Cruz PM, Yasumura D, Weir J, et al. Mutation of the receptor tyrosine kinase gene Mertk in the retinal dystrophic RCS rat. Hum Mol Genet 2000;9:645–651. [PubMed: 10699188]
16. Gal A, Li Y, Thompson DA, et al. Mutations in MERTK, the human orthologue of the RCS rat retinal dystrophy gene, cause retinitis pigmentosa. Nat Genet 2000;26:270–271. [PubMed: 11062461]
17. Finnemann SC, Bonilha VL, Marmorstein AD, Rodriguez-Boulan E. Phagocytosis of rod outer segments by retinal pigment epithelial cells requires alpha(v)beta5 integrin for binding but not for internalization. Proc Natl Acad Sci USA 1997;94:12932–12937. [PubMed: 9371778]
18. Finnemann SC, Silverstein RL. Differential roles of CD36 and alphavbeta5 integrin in photoreceptor phagocytosis by the retinal pigment epithelium. J Exp Med 2001;194:1289–1298. [PubMed: 11696594]
19. Finnemann SC. Role of alphavbeta5 integrin in regulating phagocytosis by the retinal pigment epithelium. Adv Exp Med Biol 2003;533:337–342. [PubMed: 15180282]
20. Young RW. A difference between rods and cones in the renewal of outer segment protein. Invest Ophthalmol 1969;8:222–231. [PubMed: 5777484]
21. Anderson DH, Fisher SK. Disc shedding in rodlike and conelike photoreceptors of tree squirrels. Science 1975;187:953–955. [PubMed: 1145180]
22. Anderson DH, Fisher SK, Steinberg RH. Mammalian cones: disc shedding, phagocytosis, and renewal. Invest Ophthalmol Vis Sci 1978;17:117–133. [PubMed: 415019]
23. Anderson DH, Fisher SK. The relationship of primate foveal cones to the pigment epithelium. J Ultrastruct Res 1979;67:23–32. [PubMed: 109622]
24. Anderson DH, Fisher SK, Erickson PA, Tabor GA. Rod and cone disc shedding in the rhesus monkey retina: a quantitative study. Exp Eye Res 1980;30:559–574. [PubMed: 7409012]
25. Fisher SK, Pfeffer BA, Anderson DH. Both rod and cone disc shedding are related to light onset in the cat. Invest Ophthalmol Vis Sci 1983;24:844–856. [PubMed: 6683265]
26. Jackson GR, Owsley C, Curcio CA. Photoreceptor degeneration and dysfunction in aging and age-related maculopathy. Ageing Res Rev 2002;1:381–396. [PubMed: 12067593]
27. Léveillard T, Mohand-Said S, Lorentz O, et al. Identification and characterization of rod-derived cone viability factor. Nat Genet 2004;36:755–759. [PubMed: 15220920]
28. Finnemann SC, Leung LW, Rodriguez-Boulan E. The lipofuscin component A2E selectively inhibits phagolysosomal degradation of photoreceptor phospholipid by the retinal pigment epithelium. Proc Natl Acad Sci USA 2002;99:3842–3847. [PubMed: 11904436]
29. Jeon CJ, Strettoi E, Masland RH. The major cell populations of the mouse retina. J Neurosci 1998;18:8936–8946. [PubMed: 9786999]
30. Szel A, Rohlich P. Two cone types of rat retina detected by anti-visual pigment antibodies. Exp Eye Res 1992;55:47–52. [PubMed: 1397129]
31. Kryger Z, Galli-Resta L, Jacobs GH, Reese BE. The topography of rod and cone photoreceptors in the retina of the ground squirrel. Vis Neurosci 1998;15:685–691. [PubMed: 9682870]
32. Blanks JC, Johnson LV. Specific binding of peanut lectin to a class of retinal photoreceptor cells: a species comparison. Invest Ophthalmol Vis Sci 1984;25:546–557. [PubMed: 6715128]
33. Hendrickson A, Hicks D. Distribution and density of medium- and short-wavelength selective cones in the domestic pig retina. Exp Eye Res 2002;74:435–444. [PubMed: 12076087]
34. Mears AJ, Kondo M, Swain PK, et al. Nrl is required for rod photoreceptor development. Nat Genet 2001;29:447–452. [PubMed: 11694879]

35. Daniele LL, Lillo C, Lyubarsky AL, et al. Cone-like morphological, molecular, and electrophysiological features of the photoreceptors of the Nrl knockout mouse. Invest Ophthalmol Vis Sci 2005;46:2156–2167. [PubMed: 15914637]
36. Challet E, Pitrosky B, Sicard B, Malan A, Pevet P. Circadian organization in a diurnal rodent, *Arvicanthis ansorgei* Thomas 1910: chronotypes, responses to constant lighting conditions, and photoperiodic changes. J Biol Rhythms 2002;17:52–64. [PubMed: 11837949]
37. Hicks D, Molday RS. Differential immunogold-dextran labeling of bovine and frog rod and cone cells using monoclonal antibodies against bovine rhodopsin. Exp Eye Res 1986;42:55–71. [PubMed: 2420630]
38. Zhu X, Brown B, Li A, Mears AJ, Swaroop A, Craft CM. GRK1-dependent phosphorylation of S and M opsins and their binding to cone arrestin during cone phototransduction in the mouse retina. J Neurosci 2003;23:6152–6160. [PubMed: 12853434]
39. Zhu X, Li A, Brown B, Weiss ER, Osawa S, Craft CM. Mouse cone arrestin expression pattern: light induced translocation in cone photoreceptors. Mol Vis 2002;8:462–471. [PubMed: 12486395]
40. Redmond TM, Yu S, Lee E, et al. Rpe65 is necessary for production of 11-cis-vitamin A in the retinal visual cycle. Nat Genet 1998;20:344–351. [PubMed: 9843205]
41. Kelley MW, Turner JK, Reh TA. Ligands of steroid/thyroid receptors induce cone photoreceptors in vertebrate retina. Development 1995;121:3777–3785. [PubMed: 8582287]
42. Szel A, Rohlich P, Van Veen T. Short-wave sensitive cones in the rodent retinas. Exp Eye Res 1993;57:503–505. [PubMed: 8282037]
43. Biel M, Seeliger M, Pfeifer A, et al. Selective loss of cone function in mice lacking the cyclic nucleotide-gated channel CNG3. Proc Natl Acad Sci USA 1999;96:7553–7557. [PubMed: 10377453]
44. Usukura J, Khoo W, Abe T, Breitman ML, Shinohara T. Cone cells fail to develop normally in transgenic mice showing ablation of rod photoreceptor cells. Cell Tissue Res 1994;275:79–90. [PubMed: 8118849]
45. Xu X, Quiambao AB, Roveri L, et al. Degeneration of cone photoreceptors induced by expression of the Mas1 protooncogene. Exp Neurol 2000;163:207–219. [PubMed: 10785460]
46. Cicerone CM. Cones survive rods in the light-damaged eye of the albino rat. Science 1976;194:1183–1185. [PubMed: 996550]
47. Cortina MS, Gordon WC, Lukiw WJ, Bazan NG. Light-induced photoreceptor damage triggers DNA repair: differential fate of rods and cones. Adv Exp Med Biol 2003;533:229–240. [PubMed: 15180269]
48. Xie HQ, Adler R. Green cone opsin and rhodopsin regulation by CNTF and staurosporine in cultured chick photoreceptors. Invest Ophthalmol Vis Sci 2000;41:4317–4323. [PubMed: 11095633]
49. Semple-Rowland SL, Lee NR, Van Hooser JP, Palczewski K, Baehr W. A null mutation in the photoreceptor guanylate cyclase gene causes the retinal degeneration chicken phenotype. Proc Natl Acad Sci USA 1998;95:1271–1276. [PubMed: 9448321]
50. Traverso V, Kinkl N, Grimm L, Sahel J, Hicks D. Basic fibroblast and epidermal growth factors stimulate survival in adult porcine photoreceptor cell cultures. Invest Ophthalmol Vis Sci 2003;44:4550–4558. [PubMed: 14507904]
51. Long KO, Fisher SK, Fariss RN, Anderson DH. Disc shedding and autophagy in the cone-dominant ground squirrel retina. Exp Eye Res 1986;43:193–205. [PubMed: 3758219]
52. Li W, DeVries SH. Separate blue and green cone networks in the mammalian retina. Nat Neurosci 2004;7:751–756. [PubMed: 15208635]
53. Katona C, Smale L. Wheel-running rhythms in Arvicanthis niloticus. Physiol Behav 1997;61:365–372. [PubMed: 9089754]
54. Katona C, Rose S, Smale L. The expression of Fos within the suprachiasmatic nucleus of the diurnal rodent Arvicanthis niloticus. Brain Res 1998;791:27–34. [PubMed: 9593811]
55. Van Reeth O, Olivares E, Turek FW, Granjon L, Mocaer E. Resynchronisation of a diurnal rodent circadian clock accelerated by a melatonin agonist. Neuroreport 1998;9:1901–1905. [PubMed: 9665623]

56. Nunez AA, Bult A, McElhinny TL, Smale L. Daily rhythms of Fos expression in hypothalamic targets of the suprachiasmatic nucleus in diurnal and nocturnal rodents. J Biol Rhythms 1999;14:300–306. [PubMed: 10447310]
57. Mahoney M, Bult A, Smale L. Phase response curve and light-induced fos expression in the suprachiasmatic nucleus and adjacent hypothalamus of Arvicanthis niloticus. J Biol Rhythms 2001;16:149–162. [PubMed: 11302557]
58. Dardente H, Klosen P, Caldelas I, Pevet P, Masson-Pevet M. Phenotype of Per1- and Per2-expressing neurons in the suprachiasmatic nucleus of a diurnal rodent (Arvicanthis ansorgei): comparison with a nocturnal species, the rat. Cell Tissue Res 2002;310:85–92. [PubMed: 12242487]
59. Caldelas I, Poirel VJ, Sicard B, Pevet P, Challet E. Circadian profile and photic regulation of clock genes in the suprachiasmatic nucleus of a diurnal mammal Arvicanthis ansorgei. Neuroscience 2003;116:583–591. [PubMed: 12559113]
60. Sicard B, Maurel D, Fuminier F, Boissin J. Circadian rhythm of photosensitivity and the adaptation of reproductive function to the environment in two populations of Arvicanthis niloticus from Mali and Burkina Faso. J Reprod Fertil 1992;95:159–165. [PubMed: 1625231]
61. Szel A, Rohlich P, Caffe AR, Juliusson B, Aguirre G, Van Veen T. Unique topographic separation of two spectral classes of cones in the mouse retina. J Comp Neurol 1992;325:327–342. [PubMed: 1447405]
62. Szel A, Rohlich P, Caffe AR, van Veen T. Distribution of cone photoreceptors in the mammalian retina. Microsc Res Tech 1996;35:445–462. [PubMed: 9016448]
63. Szel A, Csorba G, Caffe AR, Szel G, Rohlich P, van Veen T. Different patterns of retinal cone topography in two genera of rodents, Mus and Apodemus. Cell Tissue Res 1994;276:143–150. [PubMed: 8187156]
64. Fatt P. Proteins of vertebrate rod outer segments: a possible role for multiple forms of rhodopsin. Exp Eye Res 1981;33:31–46. [PubMed: 7250230]
65. Molday RS, Molday LL. Identification and characterization of multiple forms of rhodopsin and minor proteins in frog and bovine rod outer segment disc membranes: electrophoresis, lectin labeling, and proteolysis studies. J Biol Chem 1979;254:4653–4660. [PubMed: 312291]
66. Feng W, Yasumura D, Matthes MT, LaVail MM, Vollrath D. Mertk triggers uptake of photoreceptor outer segments during phagocytosis by cultured retinal pigment epithelial cells. J Biol Chem 2002;277:17016–17022. [PubMed: 11861639]
67. Finnemann SC. Focal adhesion kinase signaling promotes phagocytosis of integrin-bound photoreceptors. EMBO J 2003;22:4143–4154. [PubMed: 12912913]
68. Hall MO, Prieto AL, Obin MS, et al. Outer segment phagocytosis by cultured retinal pigment epithelial cells requires Gas6. Exp Eye Res 2001;73:509–520. [PubMed: 11825022]
69. Young RW. Renewal systems in rods and cones. Ann Ophthalmol 1973;5:843–854. [PubMed: 4582806]
70. Young RW. The daily rhythm of shedding and degradation of cone outer segment membranes in the lizard retina. J Ultrastruct Res 1977;61:172–185. [PubMed: 562420]
71. Tamai M, Chader GJ. The early appearance of disc shedding in the rat retina. Invest Ophthalmol Vis Sci 1979;18:913–917. [PubMed: 478781]
72. Tamai M, Teirstein P, Goldman A, O'Brien P, Chader G. The pineal gland does not control rod outer segment shedding and phagocytosis in the rat retina and pigment epithelium. Invest Ophthalmol Vis Sci 1978;17:558–562. [PubMed: 566259]
73. Terman JS, Reme CE, Terman M. Rod outer segment disk shedding in rats with lesions of the suprachiasmatic nucleus. Brain Res 1993;605:256–264. [PubMed: 8481775]
74. Teirstein PS, Goldman AI, O'Brien PJ. Evidence for both local and central regulation of rat rod outer segment disc shedding. Invest Ophthalmol Vis Sci 1980;19:1268–1273. [PubMed: 7429763]
75. O'Day WT, Young RW. Rhythmic daily shedding of outer-segment membranes by visual cells in the goldfish. J Cell Biol 1978;76:593–604. [PubMed: 632320]
76. Young RW. The daily rhythm of shedding and degradation of rod and cone outer segment membranes in the chick retina. Invest Ophthalmol Vis Sci 1978;17:105–116. [PubMed: 624604]
77. Immel JH, Fisher SK. Cone photoreceptor shedding in the tree shrew (Tupaia belangerii). Cell Tissue Res 1985;239:667–675. [PubMed: 3986885]

78. Laird D, Molday RS. Evidence against the role of rhodopsin in rod outer segment binding to RPE cells. Invest Ophthalmol Vis Sci 1988;29:419–428. [PubMed: 3343097]

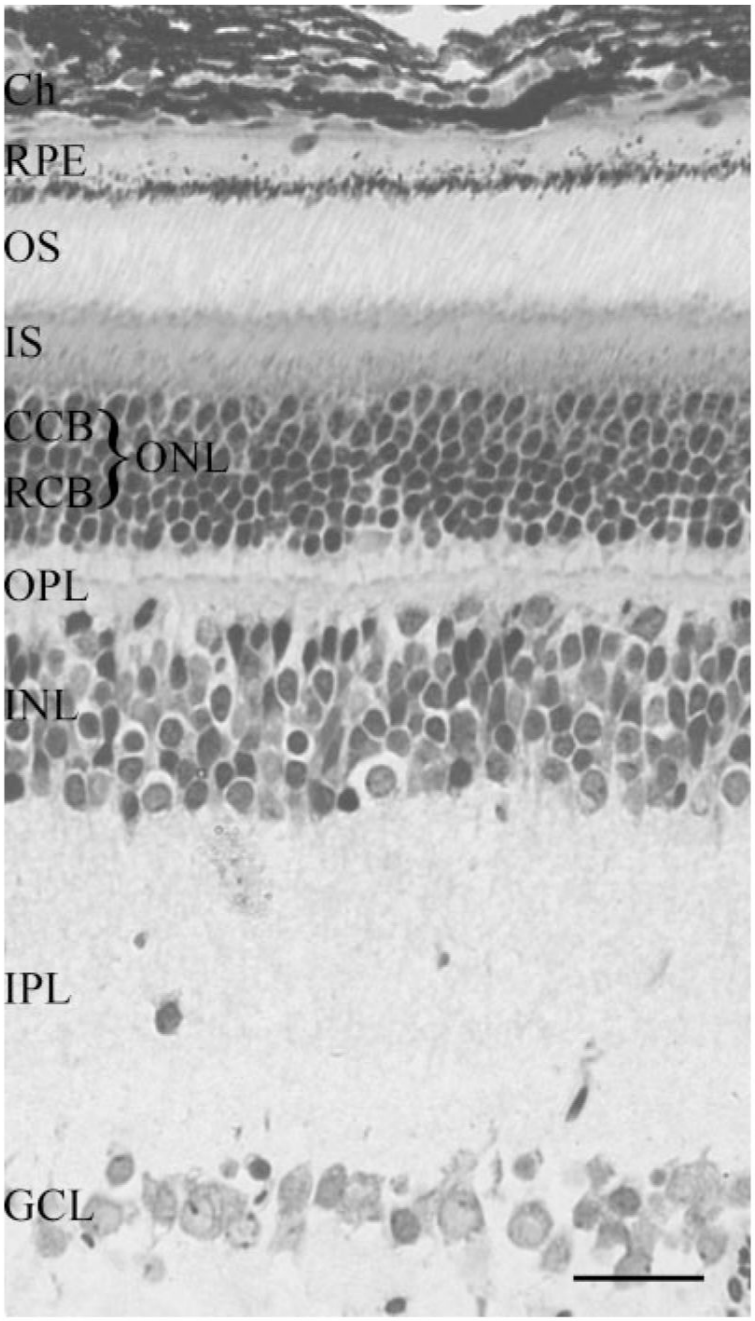


**Figure 1.**
Toluidine-blue–stained semithin section of retina from adult *A. ansorgei*. The typical layered structure of mature retina is apparent, and the more lightly stained cone nuclei are visible in the *upper rows* of the outer nuclear layer, (ONL; constituted by the cone [CCB] and rod [RCB] cell bodies). Ch, choroid; GCL, ganglion cell layer; INL, inner nuclear layer; IPL, inner plexiform layer; IS, photoreceptor inner segments; OPL, outer plexiform layer. Scale bar, 20 $\mu$m.

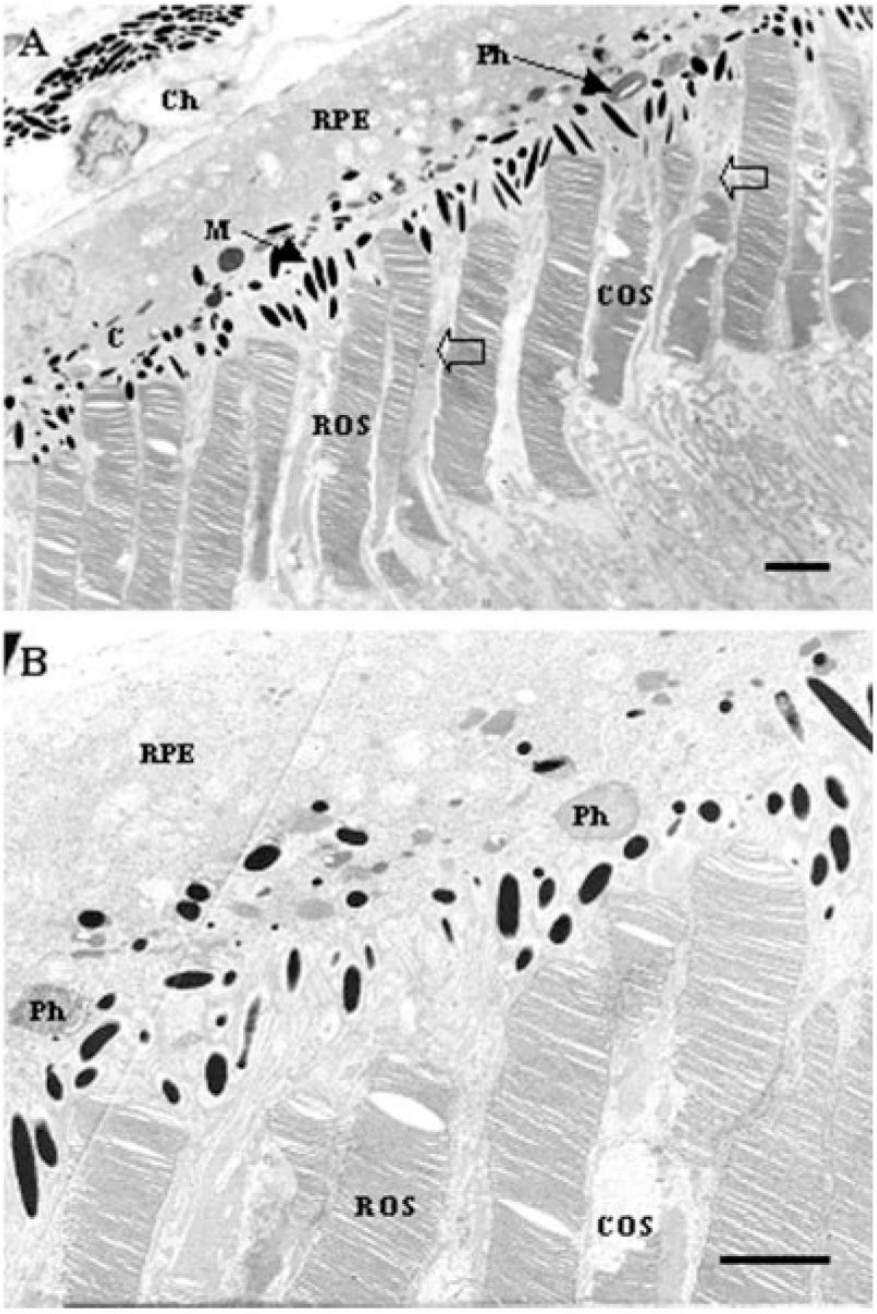


**Figure 2.**
Electron microscopic images of the PR–RPE interface in adult *A. ansorgei*. Shown are representative views of rod (ROS) and cone (COS) outer segments apposed to the RPE. COS were identified from their tapered shape and lower position, slightly greater electron density, and greater artifactual damage during tissue processing. In addition, traces of cone matrix sheath were visible surrounding them (*open arrows*). Several phagosomes (Ph) are visible within the RPE cytoplasm in both panels (tissue obtained at 0900 hours). Ch, choroid; M, melanin granules. Scale bar, 1 $\mu$m.

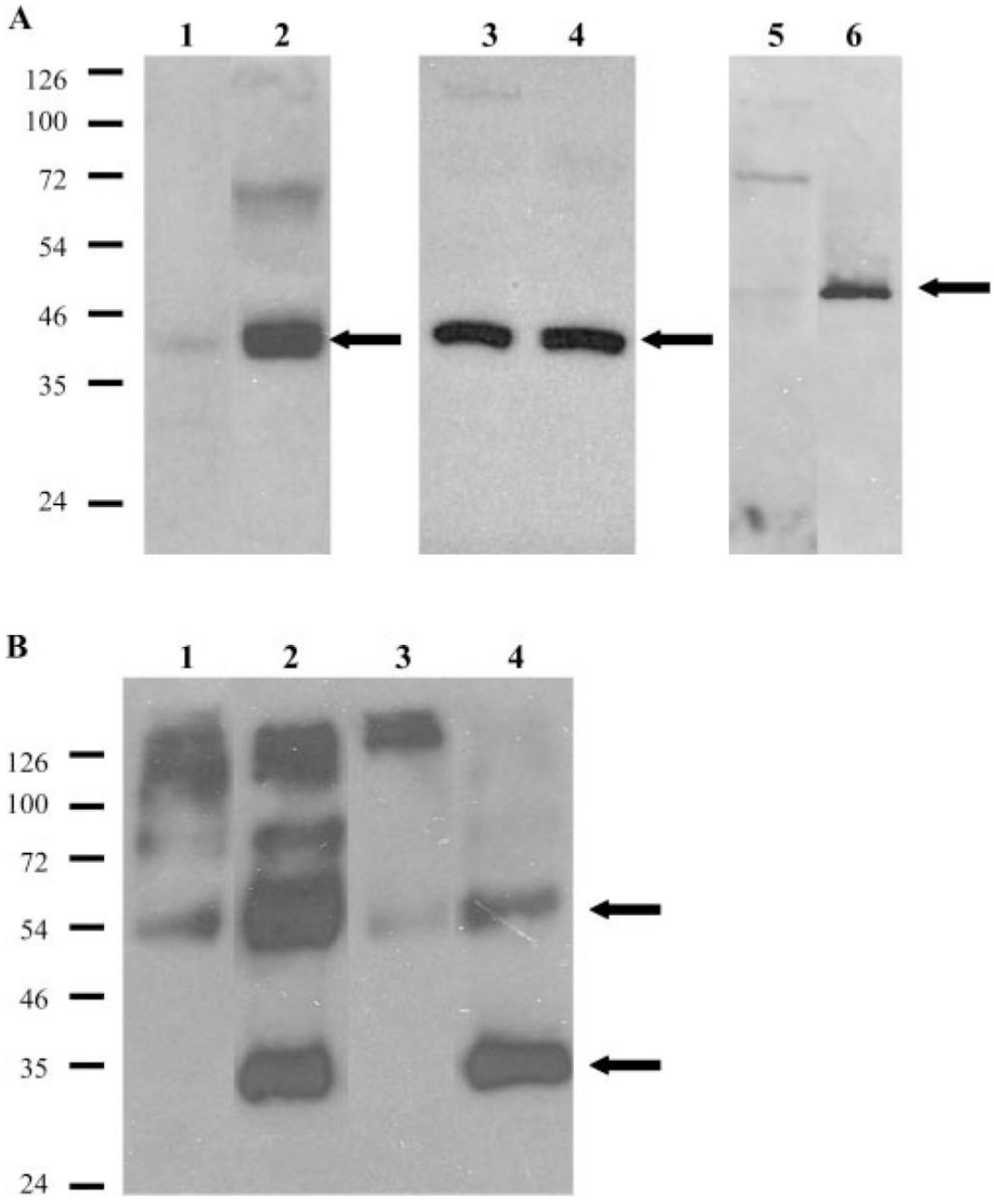


**Figure 3.**

Western blot analysis of mouse rod- and cone-specific antibodies in retinal extracts from adult *A. ansorgei* and *R. norvegicus*. Total proteins isolated from retinas of either species were run in parallel and immunoblotted with cone (**A**) or rod (**B**) antibodies. (**A**) *Lanes 1* and *2*: MW-cone opsin; *lanes 3* and *4*: SW-cone opsin; *lanes 5* and *6*: cone arrestin. *Lanes 1, 3, 5*: rat retina; *lanes 2, 4, 6: A. ansorgei* retina. Whereas immunoreactive bands were of the same apparent mass in both species, MW-cone opsin and cone arrestin were much more highly expressed in *A. ansorgei* retina. SW-cone opsin intensity was equal in both species (the blot was exposed for much longer times than the others, because of the small amount of SW-cone material). (**B**) *Lanes 1, 2*: rat retina; *lanes 3, 4: A. ansorgei* retina. *Lanes 1, 3*: boiled samples; *lanes 2,*

*4*: unheated samples. Rho-4D2 immunoreactive bands are visible at several positions corresponding to multimeric forms of rhodopsin, whereas both unheated specimens show strong monomeric bands at ~35 kDa.

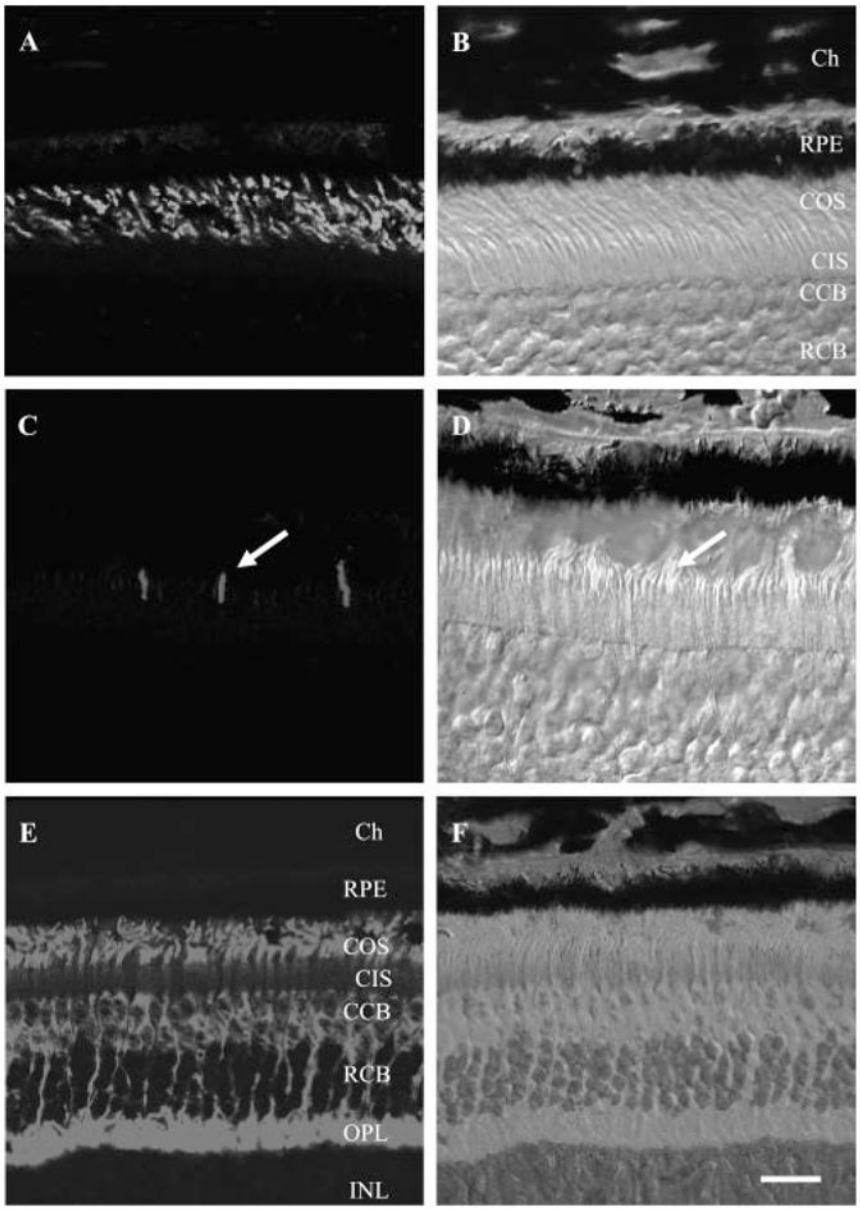


**Figure 4.**

Light microscopic immunohistochemistry of mouse cone antibodies in *A. ansorgei* retina. *Left*: immunofluorescence images; *right*: corresponding bright-field images and overlapping fluorescent signal. (**A**, **B**) MW-cone opsin; (**C**, **D**) SW-cone opsin; (**E**, **F**) cone arrestin. MW-cone opsin was present across the level of the OS, SW-cone opsin was detected on very few structures (*arrows*), and cone arrestin was very prominent throughout the cone cell bodies, from OS down to synaptic pedicle. CCB, cone cell bodies; Ch, choroid; CIS, cone inner segments; COS, cone outer segments; RCB, rod cell bodies; RPE, retinal pigmented epithelium. Scale bar: (**A**–**D**) 20 $\mu$m; (**E**, **F**) 40 $\mu$m.

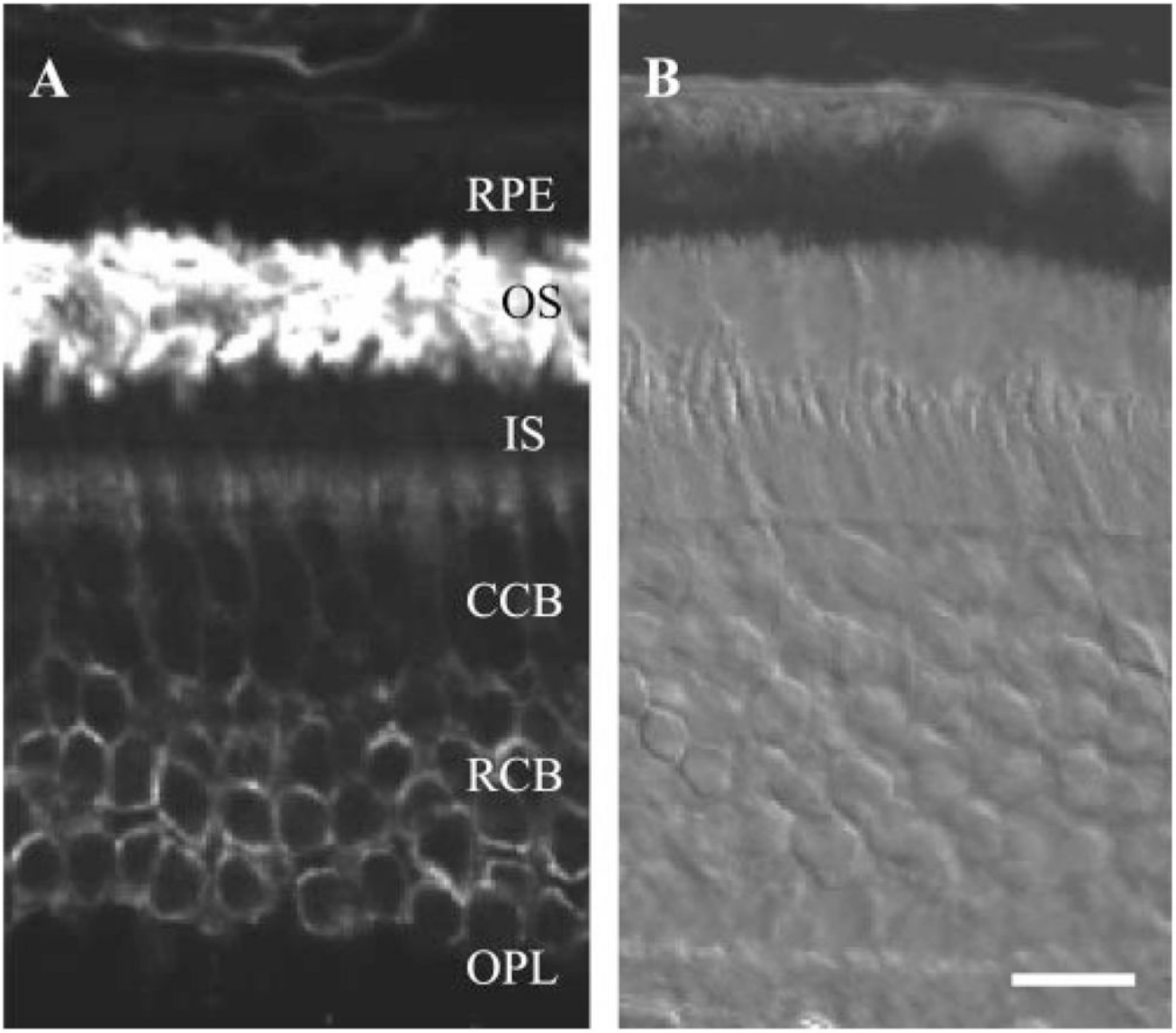


**Figure 5.**
Light microscopic immunohistochemistry of rod opsin in *A. ansorgei* retina. (**A**) Rho-4D2 stained the OS very heavily, with discrete staining of the plasma membranes of rod cell bodies (RCB) in the inner two-thirds of the outer nuclear layer. Labeling was absent from the cone cell bodies (CCB). (**B**) Nomarski image of same field. Abbreviations as in Figure 4. Scale bar, 20 $\mu$m.

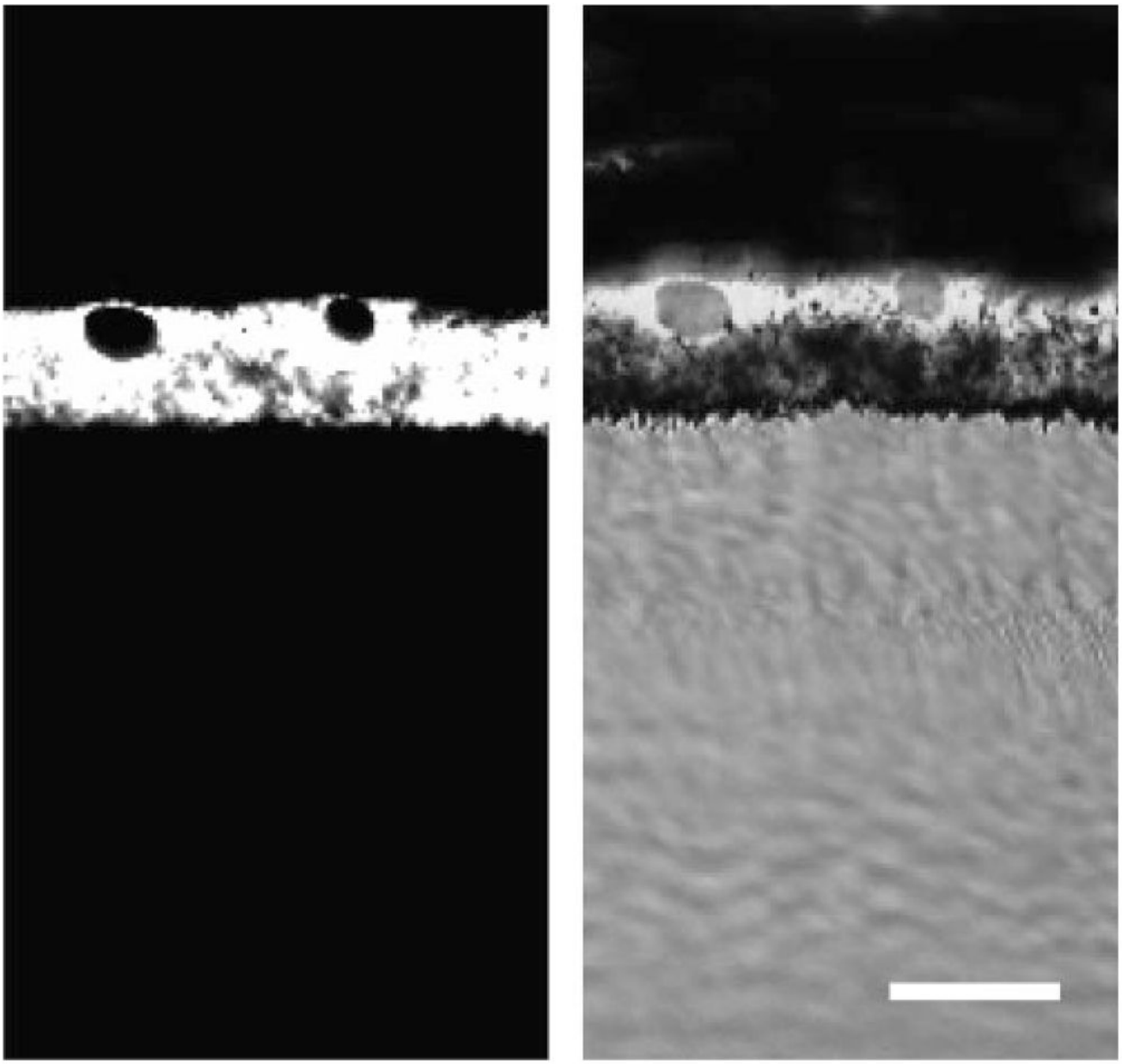

**Figure 6.**
Light microscopic immunohistochemistry of RPE65 antibody in *A. ansorgei* retina. RPE65 immunoreactivity was intense and specific within the RPE (**A**) and did not label other regions of the retina (**B**). Scale bar, 40 $\mu$m.

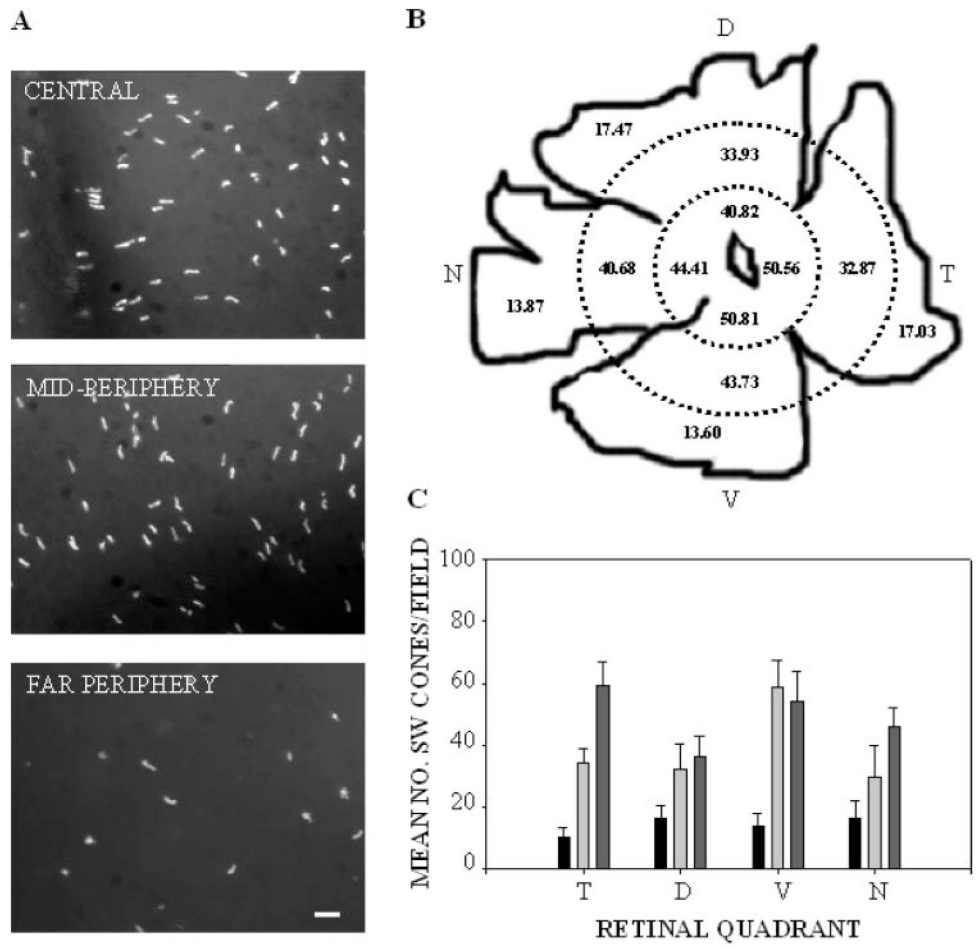


**Figure 7.**

Qualitative and quantitative immunolabeling of SW-cones in whole flatmounted *A. ansorgei* retinas. (**A**) Typical fields of SW-cones as seen in central, mid peripheral, and far peripheral areas of whole-mounted retina. Scale bar, 20 $\mu$m. (**B**) The number of SW-cones was ascertained by calculating the mean number in 18 randomly selected microscope fields within each of the 12 retinal sectors (central, mid periphery, and far periphery in each quadrant). Each field was 2250 $\mu m^2$ at a magnification of 40×. SW-cone opsin immunoreactivity was detected in uniformly scattered structures across the retinal surface. Average densities were then projected on a camera lucida representation of the whole-mount. (**C**) Histographic representation of the same data. *Black*: far periphery; *light gray*: mid periphery; *dark gray*: central retina. ANOVA followed by an ad hoc honest significant difference (HSD) test indicated no significant differences in the mean number of SW cones between left and right eyes or between any of the four quadrants. However, statistical significance was reached comparing far periphery to either mid periphery ($P = 0.00047$) or central ($P = 0.00016$), whereas mid periphery was not significantly different from central.

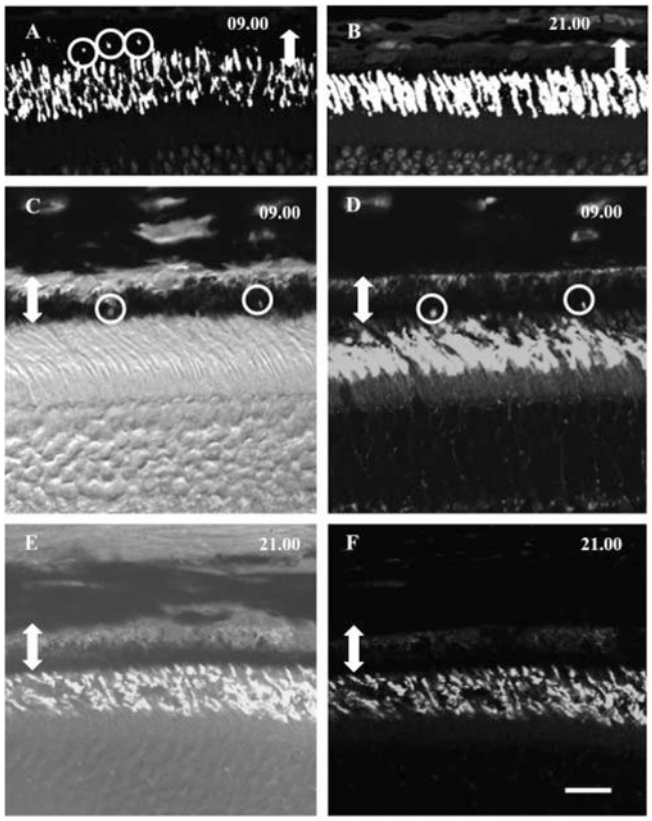


**Figure 8.**

Immunohistochemical detection of rhythmic phagocytosis in rods (**A**, **B**) and cones (**C**–**F**) of adult *A. ansorgei*. Sections taken from subjects killed at 0900 (**A**) and 2100 hours (**B**) (1 hour after lights on and lights off, respectively) and immunolabeled with rho-4D2 show the presence of numerous immunoreactive inclusions within the RPE (*circles*) at 0900 but not 2100 hours. *Double-headed arrow*: the width of the RPE. Sections taken from individuals killed at 0900 (**C**, **D**) and 2100 hours (**E**, **F**), 1 hour after lights on and lights off, respectively, and immunolabeled with MW-cone opsin showed the presence of immunoreactive inclusions at 0900 but not 2100 hours. (**C**, **E**) Merged fluorescence and bright-field images to show the position of immunoreactive phagosomes within the RPE. *Double-headed arrow*: width of the RPE. Scale bar, 15 $\mu$m.

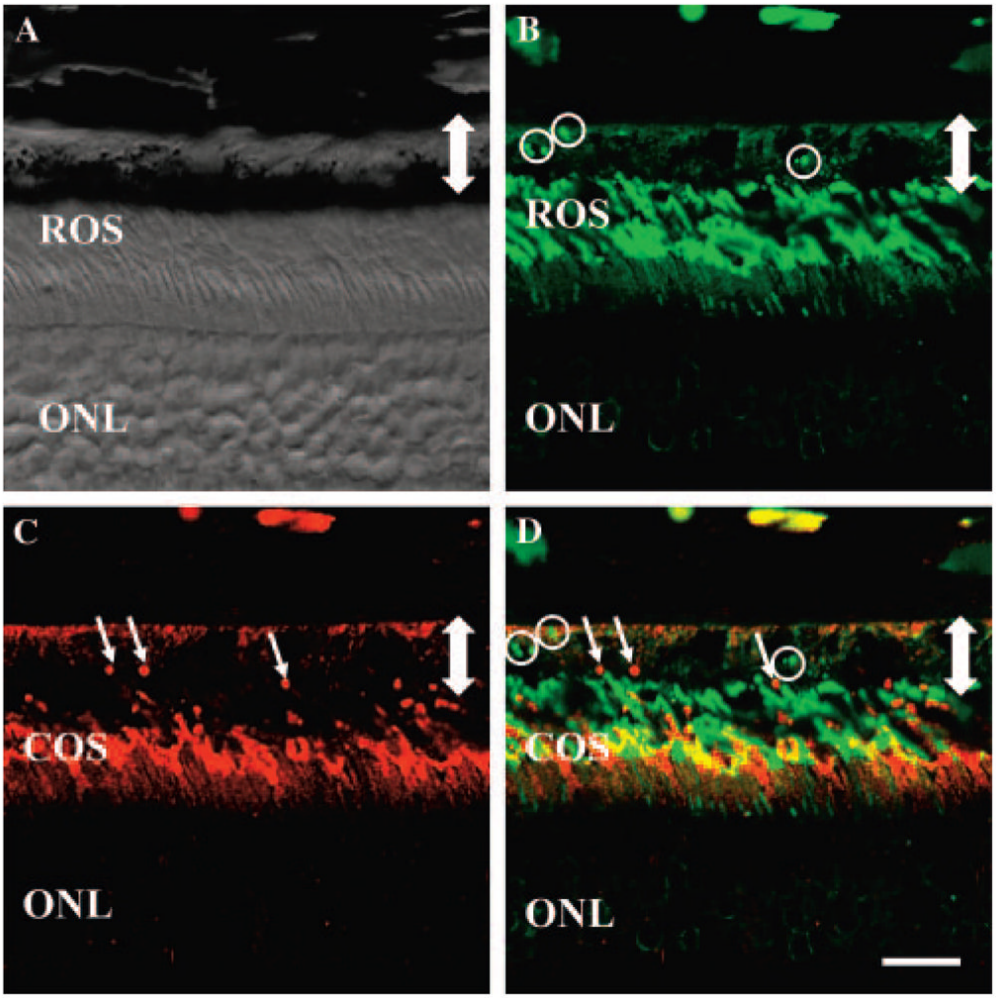


**Figure 9.**
Double-label immunohistochemistry of phagocytosis within *A. ansorgei* retina. Sections obtained at 0900 hours were stained with rho-4D2 (*green*) and MW-cone opsin antibody (*red*). (**A**) Bright-field image showing the outer retina and RPE; (**B**) rho-4D2 labeling of the same field, including several immunopositive phagosomes (*circles*); (**C**) MW-cone opsin labeling of the same field, including several immunopositive phagosomes (*short arrows*); (**D**) merged image of (**B**) and (**C**), showing presence of both rod and MW-cone phagosomes in the RPE. *Double-headed arrow*: width of the RPE. ONL, outer nuclear layer; COS, cone outer segments; ROS, rod outer segments. Scale bar, 15 $\mu$m.

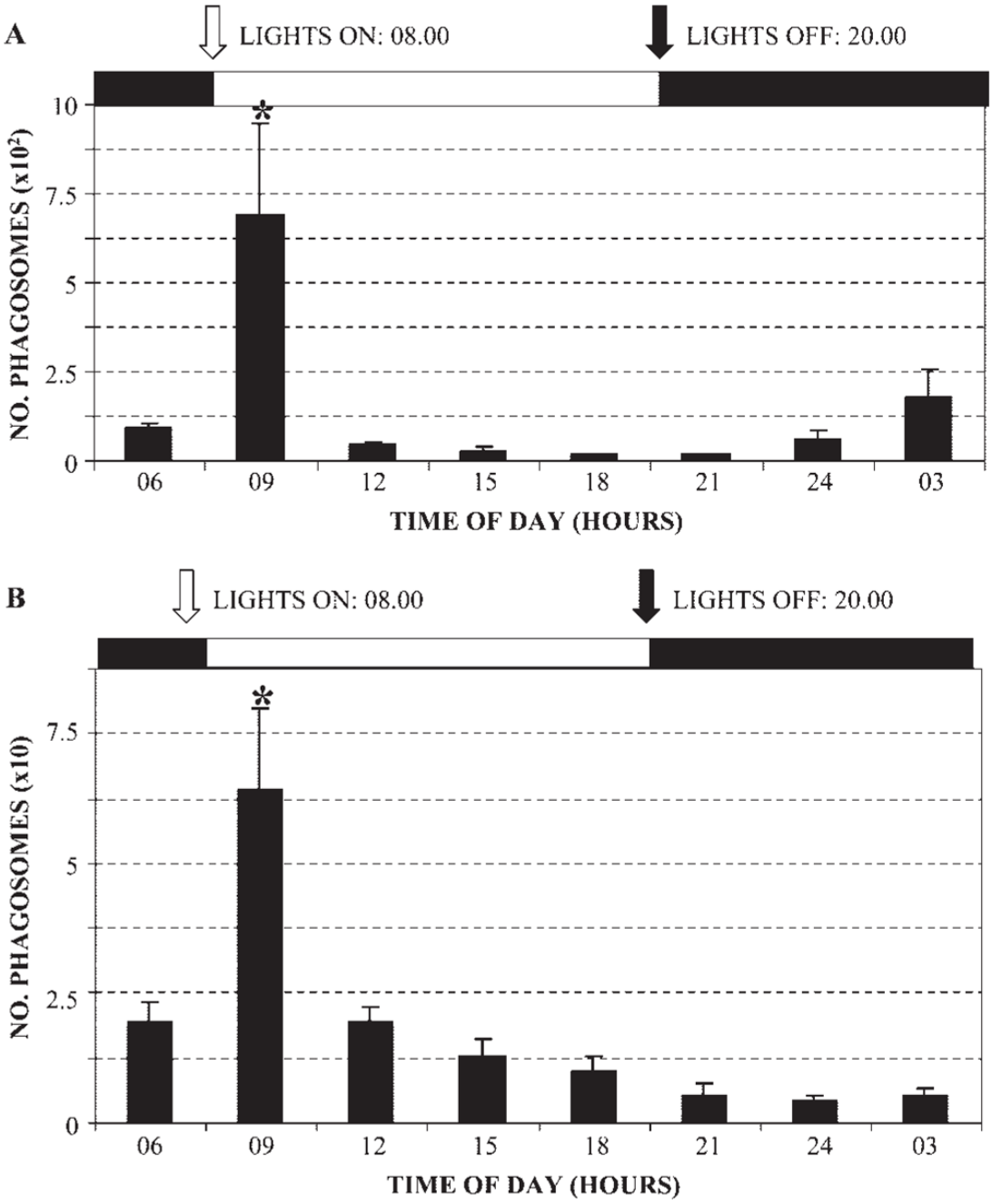


**Figure 10.**

Quantitative analysis of rhythmic rod and cone phagocytosis in adult *A. ansorgei*. Phagosome counts were made every 3 hours throughout both the light and dark periods. (**A**) Rod phagocytosis: as seen in other species, a large burst in the number of rod phagosomes was seen 1 hour after light onset, significantly different from all other values ($P < 0.0001$). Phagosome numbers were lowest in late daytime, but showed a smaller but noticeable peak late at night. (**B**) Cone phagocytosis: similar to the kinetic profile for rods, cone phagocytosis peaked shortly after light onset, but the order of magnitude was always 10 times lower than that of rods (note difference in *y*-axis scales).

**Table 1**

Total Data from All Individuals Counted during the Experiments Shown in Figure 10

| | Time of Day (24-h Clock) | | | | | | | |
|---|---|---|---|---|---|---|---|---|
| | **0600** | **0900** | **1200** | **1500** | **1800** | **2100** | **2400** | **0300** |
| **Animal** | **N** | **D** | **D** | **D** | **D** | **N** | **N** | **N** |
| 1 | | | | | | | | |
| Age (mo) | 7 | 18 | 6 | 5 | 5 | 5 | 7 | 19 |
| Rod phagosomes | 102 | 1309 | 50 | 28 | 15 | 29 | 26 | 181 |
| Cone phagosomes | 24 | 43 | 25 | 15 | 7 | 9 | 2 | 9 |
| 2 | | | | | | | | |
| Age (mo) | 7 | 6 | 6 | 5 | 5 | 5 | 7 | 16 |
| Rod phagosomes | 97 | 878 | 56 | 57 | 26 | 12 | 12 | 402 |
| Cone phagosomes | 28 | 38 | 22 | 21 | 5 | 2 | 4 | 5 |
| 3 | | | | | | | | |
| Age (mo) | 7 | 6 | 6 | 5 | 5 | 5 | 7 | 26 |
| Rod phagosomes | 108 | 445 | 59 | 13 | 20 | 14 | 127 | 29 |
| Cone phagosomes | 15 | 69 | 12 | 9 | 10 | 1 | 4 | 3 |
| 4 | | | | | | | | |
| Age (mo) | 7 | 6 | 6 | 5 | 5 | 5 | 7 | 26 |
| Rod phagosomes | 66 | 122 | 24 | 15 | 14 | 21 | 69 | 86 |
| Cone phagosomes | 11 | 107 | 20 | 5 | 18 | 9 | 7 | 4 |

Data are replotted as time of day (0900–1800 represent daylight, D; 2100–0600 represent nighttime, N with average phagosome count from all four sections for a given individual. Also given are the ages of each animal. This representation illustrates the variation that was recorded between individuals for a given time point, and the inverse correlation between phagosome number and age.